Zhang RS, Quan WZ, Fan LB *et al.* Distinguishing computer-generated images from natural images using channel and pixel correlation. JOURNAL OF COMPUTER SCIENCE AND TECHNOLOGY 35(3): 592–602 May 2020. DOI 10.1007/s11390-020-0216-9

Distinguishing Computer-Generated Images from Natural Images Using Channel and Pixel Correlation

Rui-Song Zhang[1,2], Wei-Ze Quan[1,2], Lu-Bin Fan[3], Li-Ming Hu[4], and
Dong-Ming Yan[1,2,4,*], *Senior Member, CCF, Member, ACM, IEEE*

[1] *National Laboratory of Pattern Recognition, Institute of Automation, Chinese Academy of Sciences, Beijing 100190, China*
[2] *School of Artificial Intelligence, University of Chinese Academy of Sciences, Beijing 100049, China*
[3] *Alibaba Group, Hangzhou 310023, China*
[4] *State Key Laboratory of Hydro-Science and Engineering, Tsinghua University, Beijing 100084, China*

E-mail: zhangruisong2019@ia.ac.cn; qweizework@gmail.com; lubin.flb@alibaba-inc.com; gehu@tsinghua.edu.cn
yandongming@gmail.com

Received December 10, 2019; revised January 5, 2020.

Abstract With the recent tremendous advances of computer graphics rendering and image editing technologies, computer-generated fake images, which in general do not reflect what happens in the reality, can now easily deceive the inspection of human visual system. In this work, we propose a convolutional neural network (CNN)-based model to distinguish computer-generated (CG) images from natural images (NIs) with channel and pixel correlation. The key component of the proposed CNN architecture is a self-coding module that takes the color images as input to extract the correlation between color channels explicitly. Unlike previous approaches that directly apply CNN to solve this problem, we consider the generality of the network (or subnetwork), i.e., the newly introduced hybrid correlation module can be directly combined with existing CNN models for enhancing the discrimination capacity of original networks. Experimental results demonstrate that the proposed network outperforms state-of-the-art methods in terms of classification performance. We also show that the newly introduced hybrid correlation module can improve the classification accuracy of different CNN architectures.

Keywords natural image, computer-generated image, channel and pixel correlation, convolutional neural network

1 Introduction

Natural images (NIs), captured by digital cameras, can accurately and objectively record the real-world scenes and are considered as an important carrier of visual information. In our daily life, NIs are often used for the accurate dissemination of news and the effective recording of evidence. Because of the strong artistic and realistic expression, computer-generated (CG) images are also an important carrier of visual information. With the advances in computer graphics rendering techniques, it becomes much easier to generate CG images with strong photorealism. It becomes more and more difficult to distinguish CG images from NIs by naked human eyes, as shown in Fig.1. Although CG images sometimes can give good visual experience, they also potentially bring security problems to news and justice.

Consequently, distinguishing CG images from NIs has become an important research problem in multimedia security and visual media processing community. To address this problem, a lot of efforts have been made using the standard machine learning framework [2–7],

Regular Paper

This work was supported by the National Key Research and Development Program of China under Grant No. 2019YFB2204104, the Beijing Natural Science Foundation of China under Grant No. L182059, the National Natural Science Foundation of China under Grant Nos. 61772523, 61620106003, and 61802406, Alibaba Group through Alibaba Innovative Research Program, and the Joint Open Research Fund Program of State Key Laboratory of Hydroscience and Engineering and Tsinghua-Ningxia Yinchuan Joint Institute of Internet of Waters on Digital Water Governance.

*Corresponding Author

which usually consists of two stages: manually designing discriminative features and training the classifiers. These hand-crafted features more or less depend on human prior knowledge and sometimes can achieve limited performance, especially for complex datasets. Considering the strong learning capacity and unified "end-to-end" optimization of convolutional neural network (CNN), recent approaches proposed CNN-based models [1, 8–12] to distinguish CG images from NIs, and achieved better detection performance compared with classic approaches [2–7]. However, the generality of the CNNs, or the module of a network, i.e., a module can be directly combined with existing CNN-based models and further improve their performance, is rarely considered in previous work.

(a) (b)

Fig.1. Two pairs of images about landscape and architecture. (a) Computer-generated images. (b) Nature images. These images are from the SPL2018 dataset [1].

In this paper, we propose a new "end-to-end" CNN architecture to address this problem. We expose different characteristics between NIs and CG images using the channel and pixel correlation information. A self-coding module is designed to deeply explore the correlation among three color channels, and then several convolutional layers without pooling operation are applied to better extract the correlation between image pixels. The newly designed network is called ScNet (Self-coding Network). The main contributions of our work include the followings.

• We design a self-coding module at the beginning of the CNN to explicitly extract correlation information between image color channels and thus enhance the discrimination capacity of the whole CNN model. Experimental results show that our proposed CNN model outperforms the state-of-the-art methods in terms of classification performance.

• We combine the proposed self-coding module with consecutive convolutional layers (without pooling operation) to extract the low-level features of input images, and this subnetwork can be directly installed in the beginning of other existing CNN models. Consequently, the performance of these existing CNN models is further improved, which validates the generality of our designed ScNet.

The rest of the paper is organized as follows. Section 2 discusses relevant existing literature, including hand-crafted feature based and deep learning based methods. Section 3 presents the motivation and details of our proposed network. Section 4 validates our network design and compares it with state-of-the-art approaches. Section 5 explains the self-coding module via advanced visualization techniques. Section 6 draws the conclusions.

2 Related Work

Existing approaches for distinguishing CG images from NIs mainly can be classified into two categories: hand-crafted feature based approaches and deep model based approaches. The former usually involves designing hand-crafted features (in either the spatial domain or a transformed domain) and training the classifiers (e.g., support vector machine (SVM)). The latter often follows a generic "end-to-end" framework by using deep neural networks.

2.1 Methods Based on Hand-Crafted Features

Several hand-crafted feature based approaches have been proposed to distinguish CG images from NIs. Based on the differences in the generation process of NIs and CG images in target models, light transmission, and acquisition methods, Ng *et al.* [2] proposed to identify CG images using features aided by fractal and differential geometry. Lyu and Farid [3] proposed a feature by combining first-order and higher-order wavelet statistics to distinguish between photographic and photorealistic images. Chen *et al.* [4] designed the feature using the statistical moments of wavelet characteristic function in the HSV color space. Gallagher and Chen [5] captured the original decoding traces of photographic images to separate CG images from NIs and achieved a good detection performance. Based on the previous studies, Sankar *et al.* [6] proposed a combination of features, including periodic correlation based features [13], color histogram features[14], momentum-based statistical features in YCbCr color space[4], and local patch statistical features[2]. From the image perception perspective, Pan *et al.*[15] proposed the discriminative features are derived from fractal dimension and several generalized dimensions to respectively capture the difference in color and the detailed texture between CG images and NIs. Zhang *et al.*[16] proposed a method based on the statistical property of local image edge patches. Li *et al.*[17] explored a local texture descriptor, i.e., uniform gray-scale invariant local binary patterns (LBP)[18], to classify NIs and CG images. Peng *et al.*[7] extracted the residuals of images after Gaussian low-pass filtering using the linear regression model, and then combined histogram statistics and multi-fractal spectrum of the residuals with the fitness of regression model as features to distinguish natural images (NIs) from rendered images. Above approaches usually achieve a good performance on the relatively simple datasets, but they often exhibit limited performance in complex and challenging datasets.

2.2 Methods Based on Deep Learning

More recently, considering the powerful learning capacity of deep neural networks[19–21], some deep-model based methods were proposed to solve this security problem. Rahmouni *et al.*[8] developed a special pooling layer to extract the statistical quantities from the convoluted images, and this can be optimized in an "end-to-end" CNN framework to distinguish computer-generated graphics from real photographic images. Quan *et al.*[10] proposed a method of adding cascaded filtering layer on the top of CNN to improve network performance. This network structure can be simply adjusted to the input of different patch sizes, and the Maximal Poisson-disk Sampling (MPS) method[22] was used to assist patch augmentation process. In addition, the authors[10] tried to provide insights into improving the photorealism of rendered images and synthesized images[23] via understanding the learned deep model. Yao *et al.*[11] proposed an approach to separating CG images from NIs based on sensor mode noise and deep learning. For the input images, three high-pass filters (HPFs) were used to remove the low-frequency signal representing image content and eliminate the interference of image content to the discrimination. He *et al.*[1] combined CNN and recursive neural network (RNN) to classify CG images and NIs. They used pre-processing operations of color space transformation and Schmid filtering to extract color and texture features. A dual-path CNN was designed to combine the color and texture feature representation of each patch and conduct global modeling of local feature representation via the directed acyclic graph RNN. Nguyen *et al.*[12] extended the application of the capsule network[24,25] to identify the CG images. Recently, Tarianga *et al.*[26] proposed an attention-based deep convolutional recurrent model to classify computer-generated images and NIs.

To the best of our knowledge, there is no existing work that considers the "generality" of the CNNs (or the module of a network). Our first study in this direction can effectively improve the classification performance of existing deep models. In this work, we design a self-coding module based on the channel correlation, and then combine consecutive convolutional layers to construct a generality-well subnetwork.

3 Proposed Method

In this section, we first explain the motivation of our method and then illustrate the proposed network architecture, which involves channel correlation module, pixel correlation module, feature fusion, and final decision.

3.1 Motivation

During the process of producing photographic images, the light collected by commercial digital cameras is filtered by the Color Filter Array (CFA) before reaching the camera sensor. Each pixel of the filtered Bayer image contains only part of the spectrum [one primary color in red (R), green (G), and blue (B)], which causes two thirds of the color information in the digital image to be lost. To obtain the complete digital color image, the sensor successively interpolates the known color in the neighborhood to estimate the missing color information of each pixel. This step leaves the correlation at the pixel and the channel level. Because CG images are generated by the rendering program instead of interpolation, these two levels of correlation may be weak in CG images. Therefore, pixel neighbor correlation and channel correlation can be used as important evidence to distinguish CG images from NIs.

Convolution operation can extract pixel correlation in the window of the convolutional kernel. However, a feature map is obtained by the direct summation of multiple convolutional channels (the process of convolution operation in CNNs), which may destroy the correlation between image color channels to some extent. Image channel correlation has attracted attention in the field of visual media security. For example, Yan *et al.*[27] used differential images, i.e., the differential between two color channels, to aid the identification of recolored images. Although the differential image is a representation of channel correlation, it does not necessarily depict the optimal correlation. To fully explore the correlation among R, G, and B channels, we design a module for the convolutional neural network to automatically learn such channel correlation.

3.2 Network Architecture

In the following, we describe the structure, operation, and mechanism of each module in the proposed network.

3.2.1 Channel Correlation

As shown in the bottom of Fig.2, we design a self-coding module with the 1×1 convolution of output channel 1 (the pink block) to explicitly learn channel correlation of input image patches. This self-coding channel correlation module is called as Conv1 module. The coefficient $[w_1, w_2, w_3]$ of 1×1 convolutional kernel represents the weights of R, G, and B channels in this correlation. This convolution operation can be expressed as

$$C_{ij} = w_1 \times R_{ij} + w_2 \times G_{ij} + w_3 \times B_{ij},$$

where C_{ij} is the pixel-wise output of the Conv1 module. When the coefficient is $[1, -1, 0]$, $[1, 0, -1]$, $[0, 1, -1]$ or other special cases, it can be regarded as learning the differential image. Compared with the hard-coding operation of the differential image, e.g., R-G in [27], the module designed by us learns the weights of the three channels and has a larger parameter space to model channel correlation in a more flexible manner. As reported in Subsection 4.2, the performance of adding three Conv1 modules is better than that of three hard-coding differential branches.

3.2.2 Pixel Correlation

After the Conv1 module, the color channel correlation of NIs and CG images is modeled. To extract the correlation between neighboring pixels, we use three 3×3 convolutions of output channel 8 without any pooling operation. Each convolution can subtly extract the correlation of nine pixels in the local neighbor patch, and the output of the convolution is formulated as

$$O_{ij} = \sum_{u=-1}^{1} \sum_{v=-1}^{1} F(u, v) \times I^k(i + u, j + v),$$

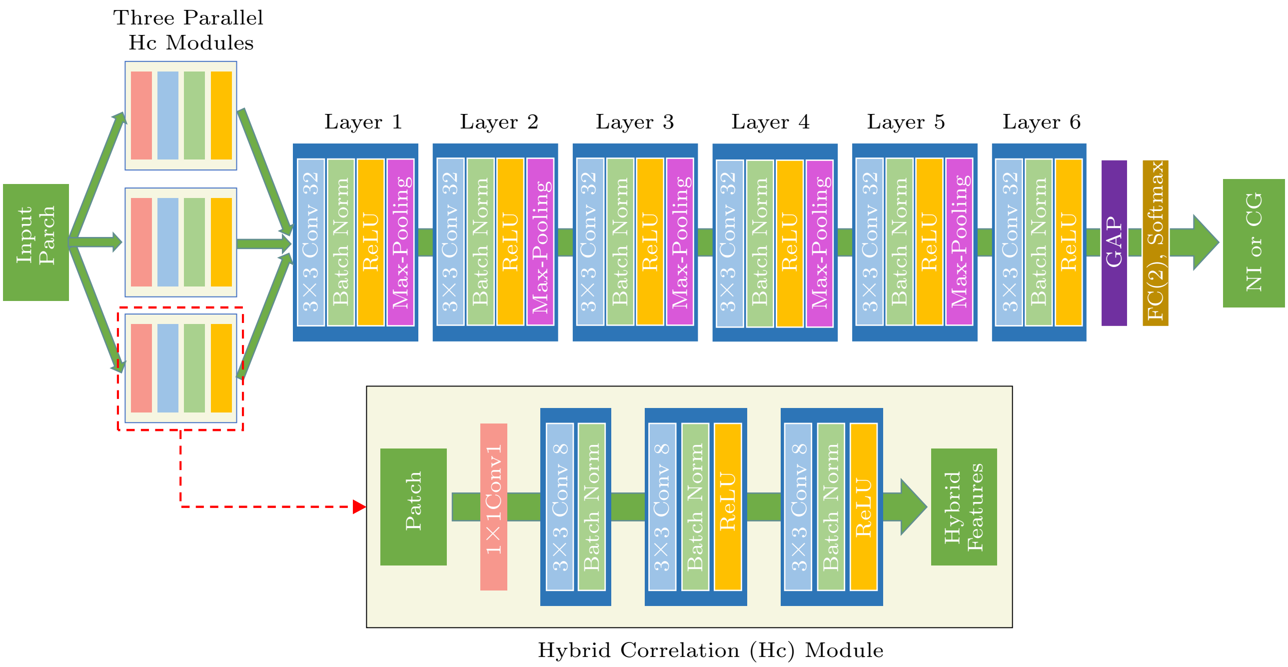

Fig.2. Architecture of our network ScNet and the hybrid correlation module. The network input is a 96×96 image patch, and the output is the label (NI or CG). Each convolutional layer shows the kernel size and the number of feature maps, e.g., "3×3 Conv 32" means the kernel size is 3×3 and the number of output channels is 32.

where F stands for the 3×3 convolutional kernels and I^k stands for the k-th channel of the input of the convolutional layer. There is no pooling operation for all three convolutional layers, so as to retain the original useful information as much as possible. We call the combination of the Conv1 module and consecutive three convolutional layers (red dotted block in Fig.2) as the hybrid correlation module (channel and pixel correlation), which is abbreviated as Hc module hereafter.

3.2.3 *Fusion and Decision*

Considering the three color channels in the RGB image, we use three parallel Hc modules to learn the hybrid correlation of input image simultaneously (the top-left corner in Fig.2). Note that, these three Hc modules are independent, and the corresponding parameters are also not shared with each other. The three Hc modules can extract different hybrid correlation information of the input image, and then we directly concatenate the output feature maps of the Hc modules. Next, we use six convolutional layers with max-pooling to further learn the hierarchical representation (layers 1–6 in Fig.2), using the above concatenated feature maps as input. In addition, the number of output channels of each convolutional layer remains the same or increases by a power of 2 from 32 to 256. All max-pooling layers have the same kernel size of 3×3 and a stride of 2. We apply a global average pooling (GAP) operation to transform the final feature maps into a high-dimensional vector. The fully-connected (FC) layer and softmax layer perform final decision on vectors and obtain probabilities belonging to two classes (NI or CG).

4 Experimental Results

In this section, we validate the network design and the generality of the proposed Hc module by comparing it with existing corresponding counterparts. The proposed network is also compared with other representative state-of-the-art networks, i.e., LiNet [10], BSP-CNN [1], YaoNet [11], and very recent attention-based model [26]. Finally, the compression robustness and generalization of these networks are evaluated.

4.1 Experimental Setup

In this work, we use the SPL2018 dataset contributed by He *et al.* [1], which contains 6 800 NIs and 6 800 CG images. The advantage of this dataset is that CG images are obtained by more than 50 pieces of rendering software, while NIs are obtained in different environments using different models of cameras. This is close to the real-world application. Following [1], the 192×192 central region of each image is cropped. Then, these cropped image patches are randomly divided into training, validation, and testing sets (with the ratio of $10:3:4$).

In view of computational cost and fair comparison, all networks have the same input size of 96×96. In the training stage, we use a batch size of 64, including 32 NIs and 32 CG images. We randomly crop the 96×96 patch from the 192×192 image to augment the training set, and shuffle the order of the training set after each epoch. Stochastic Gradient Descent (SGD) [28] is used to optimize the parameters of CNN models. The initial learning rate is set as 0.001 and divided by 10 every 400 epochs. The training process stops after 1 200 epochs, and all test results are reported at 1 200 epochs. For the SGD optimizer, we employ a weight decay of 0.000 1 and a momentum of 0.9. In the testing stage, we follow the 10-crop average: for each test image (192×192), we crop five patches of 96×96 pixels (the center and four corner patches), flip these patches horizontally, and finally average the predictions of total 10 patches as the final result. All experiments are implemented with PyTorch 0.4.1. We train the network for 1 200 epochs, which takes about 105 minutes on a GeForce® GTX 1080Ti. In addition, all reported results are the average of three random splits.

4.2 Validation of Network Architecture Design

We evaluate our network by comparing classification accuracies of ScNet and three corresponding variants, i.e., ScNet-3Pc, ScNet-3Di, and ScNet-Base. 3Pc stands for the variant of three parallel Hc modules removing the Conv1 module ("1×1 Conv 1" in Fig.2). 3Di stands for the variant of three parallel Hc modules replacing the Conv1 module with three hard-coding differential images (R-G, R-B, and G-B) [27] respectively. Base stands for the architecture starting from "layer 1" in Fig.2. We record the training loss of above four networks for one random split and the corresponding curve is plotted in Fig.3. The training loss quickly decreases in the first 600 epochs and the network reaches the stability after about 1 000 epochs. Fig.4 shows the classification accuracies of these four networks on the validation set. Among four networks, ScNet achieves the best performance.

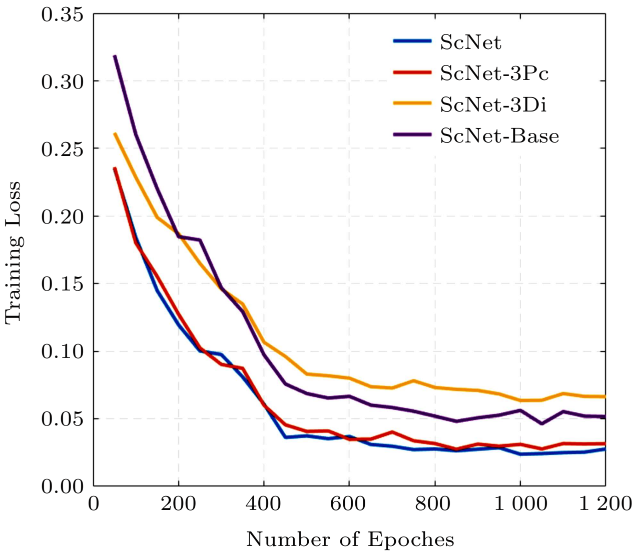

Fig.3. Training loss of ScNet and three corresponding variants.

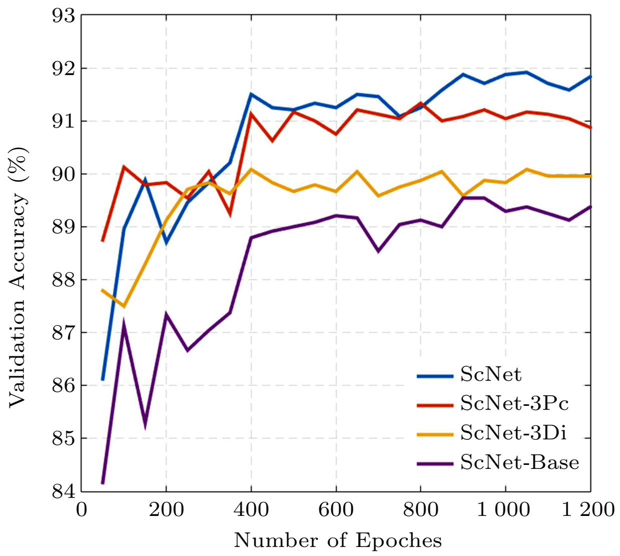

Fig.4. Accuracy rate of ScNet and three corresponding variants on the validation set.

Table 1 reports the classification accuracies of ScNet, ScNet-3Pc, ScNet-3Di, and ScNet-Base on the testing set. For clarity, the highest accuracy is in bold, and this is the same for the remaining tables. As shown in the last column of Table 1, ScNet is stably superior to the other three variants, such as ScNet-3Di and ScNet-Base by 2.01% and 1.72%, respectively. Compared with ScNet-3Pc, the average classification accuracy of ScNet is improved by 0.46%. This improvement indicates that our Conv1 module can effectively capture the correlation between image color channels, and the channel correlation information is useful for the classification of NIs and CG images. In addition, we find that our self-coding strategy for exploring the correlation information between color channels is more flexible and effective than the hard-coding strategy (see the rows of "ScNet" and "ScNet-3Di" in Table 1). In fact, the former follows the philosophy of deep learning, whereas the latter follows that of feature engineering.

Table 1. Classification Accuracies of ScNet and Three Corresponding Variants

Architecture	First (%)	Second (%)	Third (%)	AVG (%)
ScNet	**94.72**	**93.69**	**94.13**	**94.18**
ScNet-3Pc	94.31	93.34	93.51	93.72
ScNet-3Di	92.28	92.22	92.00	92.17
ScNet-Base	93.34	91.88	92.16	92.46

Note: "First", "Second", and "Third" correspond to one random split respectively. "AVG" is the average value of these three random splits.

4.3 Validation of Module Generality

From Table 1, we show that the Hc module achieves the improvement by 1.72% when comparing "AVG" of "ScNet" and "ScNet-Base". In the following, we evaluate the generality of this Hc module, i.e., the impact of combining the Hc module with existing CNN models. In this work, we consider three recent CNN models: LiNet [10], BSP-CNN [1], and YaoNet [11]. The corresponding results are reported in Table 2. The two variants of 3Hc mentioned in Subsection 4.2, i.e., 3Pc and 3Di, are also tested. In addition, "Base" in Table 2 stands for the original network designed by its authors, and the meaning of symbol "Base" is different from that mentioned in Subsection 4.2.

Table 2. Generality Evaluation of Hc Module in Three Recent CNN Models (LiNet [10], BSP-CNN [1], and YaoNet [11])

	LiNet (%)	BSP-CNN (%)	YaoNet (%)
3Hc	**93.93**	**93.34**	**93.69**
3Pc	93.57	93.14	93.28
3Di	92.02	91.99	91.70
Base	92.38	91.79	89.07

Note: "Base" stands for the original network proposed by its authors.

Comparing the rows of "3Hc" and "Base" in Table 2, we find that the classification accuracy of 3Hc (the architecture of three parallel Hc modules shown in Fig.2) for three networks is higher than that of Base by 1.55%, 1.55%, and 4.62%, respectively. This indicates that the 3Hc module can further improve the classification performance of existing networks through directly adding this hybrid correlation module at the beginning of existing networks. It is worth noting that the accuracy of 3Pc for all three networks is lower than that of 3Hc, which implies that the Conv1 module also has good generality, i.e., explicitly extracting the channel correlation information to enhance the discrimination capacity of networks. In addition, the accuracy of 3Di of LiNet is lower than that of LiNet by 0.36%, whereas this drop does not exist for BSP-CNN and YaoNet (comparing the rows of "3Di" and "Base" in Table 2) . This implies that the differential images (even similar hard-coding strategy) may be difficult to guarantee their generality, i.e., consistently and stably improving the performance of existing CNN models.

4.4 Comparison with the State of the Art

We first compare the designed ScNet with the state-of-the-art approaches. By comparing the "AVG" of "ScNet-Base" in Table 1 with the row of "Base" in Table 2, we find that the average classification accuracy of ScNet-Base (starting from "layer 1" in Fig.2) is higher than that of LiNet [10], BSP-CNN [1], and YaoNet [11], respectively. This suggests that the Base structure of ScNet can extract the correlation between patch pixels better than other networks. Compared with three recent networks adding modules of 3Hc, 3Pc, and 3Di, ScNet, ScNet-3Pc, and ScNet-3Di still show the best performance. For example, for the 3Hc module, the average classification accuracy of ScNet (the "AVG" of "ScNet" in Table 1) is higher than that of LiNet, BSP-CNN, and YaoNet (the row of "3Hc" in Table 2) by 0.25%, 0.84%, and 0.49%, respectively. It indicates that ScNet is superior to the other three networks. Furthermore, the accuracy of ScNet is 0.31% higher than the best discrimination result of 93.87% in the SPL2018 dataset reported by [1], which indicates that the network designed by us has superior discrimination performance. Note that, our ScNet is simpler than the network used in [1] where the authors combined the dual-path CNN with hand-crafted preprocessing operations and DAG-RNN.

We also compare ScNet-Base and ScNet with the latest attention-based deep convolutional recurrent model [26]. The following experiments are conducted on RAISE [29] versus PRCG [30], and the experiment setup is the same as those described in [26]. The corresponding results are reported in Table 3. The average classification accuracies for both patch and voting of ScNet-Base and ScNet are always higher than that of network proposed in [26]. In addition, the patch accuracy of ScNet (i.e., with 3Hc module) is higher than that of ScNet-Base for all patch sizes (see the column "Patch" of "ScNet" and "ScNet-Base" in Table 3). This is also consistent with previous analysis that our proposed Hc module can further improve the classification performance.

4.5 Robustness Against Post-Processing

The robustness of detection models against post-processing is important because the using of post-processing operation can weaken the statistical characteristics of CG images and NIs, so as to deceive the detectors. Here, we mainly examine the impact of JPEG compression on the identification of CG images, with compression factors from 95 to 35 with a step of 10. In the testing set, both natural samples and computer-generated samples are compressed. There is no obvious visual difference between the compressed and the uncompressed images. All the following experiments use the trained models in Subsection 4.2 and Subsection 4.3, and there is no additional training for compressed images.

Table 4 shows the statistics of the robustness test of the 3Hc structure and the Base structure in the four networks (ScNet, LiNet, BSP-CNN, and YaoNet) to JPEG compression with seven different quality factors. For each of the seven quality factors (shown in Table 4), it is always ScNet, with the 3Hc module, that has the highest accuracy expect for two cases (87.18% for LiNet-3Hc, and 87.12% for BSP-CNN-3Hc in the row of "85"). Note that, the corresponding accuracy for ScNet-3Hc is 87.07%, and it is very close to the

Table 3. Classification Accuracies of ScNet-Base, ScNet and Model in [26] on RAISE vs PRCG for Four Different Patch Sizes

Patch Size	ScNet-Base		ScNet		Tarianga *et al.* [26]	
	Patch (%)	Voting (%)	Patch (%)	Voting (%)	Patch (%)	Voting (%)
240×240	99.40	100	99.94	100	97.40	97.20
120×120	99.27	100	99.73	100	96.90	97.69
60×60	98.64	100	99.63	100	94.90	94.55
30×30	97.57	100	99.21	100	90.90	92.67

Table 4. Performance Evaluation of Four Networks with/Without 3Hc Module on the JPEG Compressed Testing Set

Quality Factor	ScNet		LiNet		BSP-CNN		YaoNet	
	3Hc (%)	Base (%)	3Hc (%)	Base (%)	3Hc (%)	Base (%)	3Hc (%)	Base (%)
-	**94.18**	92.46	93.93	92.38	93.34	91.79	93.69	89.07
95	**93.26**	91.43	92.43	91.74	92.06	91.11	91.70	87.59
85	87.07	86.73	**87.18**	86.62	87.12	86.67	86.48	82.20
75	**82.36**	82.25	81.97	79.83	80.66	81.83	82.01	79.96
65	**81.94**	78.62	77.92	75.50	80.35	78.53	80.53	77.24
55	**80.08**	76.83	76.67	72.97	78.47	76.64	77.79	74.75
45	**79.95**	76.43	76.75	71.85	78.39	76.13	77.54	73.44
35	**79.44**	76.39	76.39	71.82	77.96	76.50	77.81	72.27

Note: "-" means results on the original testing set. All models are trained on the original training set.

above two values. In addition, the accuracy of the network with 3Hc is better than that of network without 3Hc. Taking ScNet as an example, the values in the column of "3Hc" are higher than those in the column of "Base". When images are under the strong compression (quality factor starting from 75 to 35), the declining speed of the accuracy of the network with 3Hc is slower than that of the network without 3Hc. For example, the gap is 2.70% for BSP-CNN-3Hc (from 80.66% to 77.96%), while 5.33% for BSP-CNN-Base (from 81.83% to 76.50%). This observation further confirms that our proposed 3Hc module can enhance the robustness of original networks for JPEG compression.

4.6 Generalization Evaluation

To apply a CNN-based detector to the real-world scenario, the generalization performance, i.e., testing on the "unseen" dataset, is an important factor. We evaluate the generalization capability of the proposed method on the highly challenging dataset of Google versus PRCG [2], which comprises NIs and CG images of heterogeneous origins and is thus close to the real-world application. All the following experiments use the trained models in Subsection 4.2 and Subsection 4.3, and these models use the training dataset of SPL2018 [1].

Table 5 reports the classification accuracies of the 3Hc structure and the Base structure in the four networks (ScNet, LiNet, BSP-CNN, and YaoNet) on the Google versus PRCG dataset. Comparing "Base" of all four networks, we find that ScNet has the highest accuracy. Note that, for LiNet, BSP-CNN and YaoNet, "Base" refers to the network architecture reported in their papers [1, 10, 11]; therefore, this illustrates that the Base structure of ScNet (starting from "layer 1" in Fig.2) has better generalization performance. When comparing the average accuracies between "Base" and "3Hc" for four networks ("AVG" in Table 5), the accuracy increases by 3.48%, 0.95%, 4.25%, and 0.46%, respectively. This improvement shows that adding the 3Hc module can enhance the network generalization capability. Furthermore, the classification accuracy of ScNet-3Hc is the highest among all of validation networks, and this means that our proposed network holds the superior generalization capability.

5 Visualization and Understanding

To better explain the working principle of Conv1 self-coding module, we visualize the coefficient of 1×1 convolutional kernel in the Conv1 module and the feature map after Conv1 encoding.

Table 5. Generalization Performance Evaluation of Four Networks with/Without 3Hc Module on the Google vs PRCG

Architecture	ScNet		LiNet		BSP-CNN		YaoNet	
	3Hc (%)	Base (%)	3Hc (%)	Base (%)	3Hc (%)	Base (%)	3Hc (%)	Base (%)
First	**82.81**	79.38	78.31	76.94	82.19	77.75	74.50	74.62
Second	**82.44**	77.88	76.31	76.50	81.13	76.69	73.75	72.69
Third	**81.69**	79.25	78.06	76.38	81.00	77.13	74.50	74.06
AVG	**82.31**	78.83	77.56	76.61	81.44	77.19	74.25	73.79

Note: "First", "Second", and "Third" show the classification accuracies of networks trained on the SPL2018 dataset with one random split, respectively. "AVG" is the average value of these three random splits.

Fig.5 shows the color mapping image of weights of each 1×1 convolutional kernel of ScNet trained on three random splits. We find that the weights of the three Conv1 modules of each random split are roughly arranged in $(+, 0, -)$, with no fixed order, which is similar to the idea of the input differential image. In addition, we find that the absolute value of the three convolutional kernel weights is in three orders of magnitude, which are the large value (positive mapping to red, negative mapping to blue), the median value (positive mapping to orange, negative mapping to cyan) and the small value (positive and negative mapping to green). For example, in the first random split, the weight of the first Conv1 (Conv1-1) is in a small magnitude and the weight color mapping is almost green. The weight of the second Conv1 (Conv1-2) is in a medium magnitude and the non-zero weight color mapping is orange and cyan. The weight of the third Conv1 (Conv1-3) is in a large magnitude and the non-zero weight color mapping is red and blue. Comparing the Conv1 of three random splits in Fig.5, the Conv1 convolutional kernel in the first random split best conforms to the above description, and ScNet trained on the first random split achieves the best results (94.72% in the row of "ScNet" in Table 1). The indirect difference of image color channels coding in three orders of magnitude can extract richer features between channels, which enable CNN to learn features better.

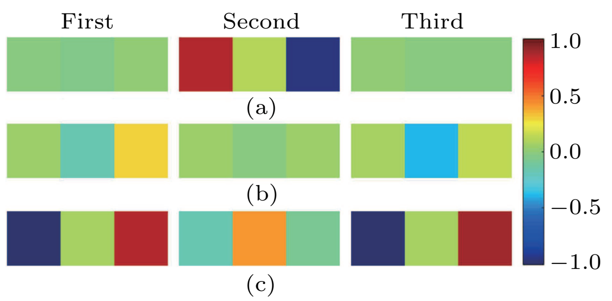

Fig. 5. Color mapping of the weights of three parallel Conv1 modules: (a) "Conv1-1", (b) "Conv1-2", and (c) "Conv1-3", for three random splits ("First", "Second" and "Third").

Fig.6 visualizes the feature maps after the Conv1 in the first random split. Fig.6(a) is a natural image (NI), and Fig.6(b) is a computer-generated image (CGI). Each column from left to right is the original input image and the respective feature map of three Conv1 modules with the weights in small, medium and large magnitude. For the NI, the words (red block of Fig.6(a)) become more and more obscure from left to right. However, the words in the CG image (red block of Fig.6(b)) are sharp for three feature maps, which is similar to [31]. The work of [31] has shown that high-frequency components across NI color channels are strongly correlated and similar. The feature maps of NI are harmonious and smooth, showing good channel correlation. The feature maps of the CG image, e.g., paint and words on the wall, are abrupt and show poor correlation. By automatically learning the correlation between color channels, the distance between NI and CG images in the feature domain is increased, and thus the network identification result is improved.

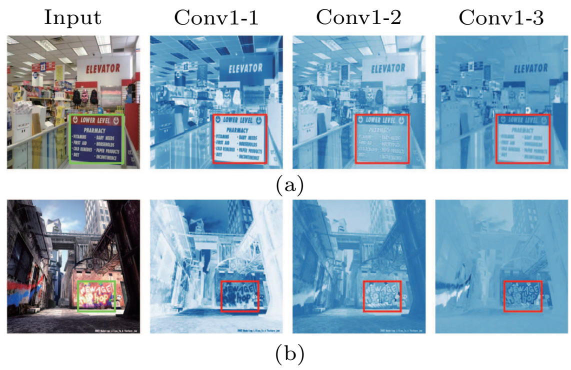

Fig.6. Feature maps on 1×1 convolutional layer of three parallel Conv1 modules in the first random split. (a) NI. (b) CGI.

6 Conclusions

In this paper, channel and pixel correlation were used to model the differences between NIs and CG images in terms of statistical characteristics. We proposed a self-coding module to extract features between image color channels and designed a CNN to better extract features between image pixels. We conducted a number of experiments to evaluate the complete framework. Compared with other advanced technologies, our framework obtained better detection performance. More importantly, the self-coding module with consecutive convolutional layers constructs a hybrid correlation module, which can be directly combined with existing CNN models, and this can further enhance their discrimination capacity. The source code of our method is attached and will be publicly released with the final version①. In future work, we would like to apply this novel framework to other multimedia security tasks, e.g., recolored image detection and image manipulation detection.

Acknowledgment We would like to thank Dr. He for kindly sharing the SPL2018 dataset [1], Dr. Dang-

①https://github.com/Evergrow/JCST_NIvsCG, May 2020.

Nguyen for the RAISE dataset [29], and Dr. Ng for the Google and PRCG dataset [30].

References

[1] He P, Jiang X, Sun T, Li H. Computer graphics identification combining convolutional and recurrent neural networks. *IEEE Signal Processing Letters*, 2018, 25(9): 1369-1373.

[2] Ng T T, Chang S F, Hsu J, Xie L, Tsui M P. Physics-motivated features for distinguishing photographic images and computer graphics. In *Proc. the 13th ACM International Conference on Multimedia*, November 2005, pp.239-248.

[3] Lyu S, Farid H. How realistic is photorealistic? *IEEE Transactions on Signal Processing*, 2005, 53(2): 845-850.

[4] Chen W, Shi Y Q, Xuan G. Identifying computer graphics using HSV color model and statistical moments of characteristic functions. In *Proc. the 2007 IEEE International Conference on Multimedia & Expo*, July 2007, pp.1123-1126.

[5] Gallagher A C, Chen T. Image authentication by detecting traces of demosaicing. In *Proc. the 2008 IEEE Conference on Computer Vision and Pattern Recognition*, June 2008.

[6] Sankar G, Zhao H V, Yang Y H. Feature based classification of computer graphics and real images. In *Proc. the IEEE International Conference on Acoustics, Speech and Signal Processing*, April 2009, pp.1513-1516.

[7] Peng F, Zhou D l, Long M, Sun X M. Discrimination of natural images and computer generated graphics based on multi-fractal and regression analysis. *AEU-International Journal of Electronics and Communications*, 2017, 71: 72-81.

[8] Rahmouni N, Nozick V, Yamagishi J, Echizen I. Distinguishing computer graphics from natural images using convolution neural networks. In *Proc. the 2017 IEEE International Workshop on Information Forensics and Security*, December 2017.

[9] Yu I, Kim D, Park J, Hou J, Choi S, Lee H. Identifying photorealistic computer graphics using convolutional neural networks. In *Proc. the IEEE International Conference on Image Processing*, September 2017, pp.4093-4097.

[10] Quan W, Wang K, Yan D M, Zhang X. Distinguishing between natural and computer-generated images using convolutional neural networks. *IEEE Transactions on Information Forensics and Security*, 2018, 13(11): 2772-2787.

[11] Yao Y, Hu W, Zhang W, Wu T, Shi Y Q. Distinguishing computer-generated graphics from natural images based on sensor pattern noise and deep learning. *Sensors*, 2018, 18(4): Article No. 1296.

[12] Nguyen H H, Yamagishi J, Echizen I. Capsule-forensics: Using capsule networks to detect forged images and videos. In *Proc. the 2019 IEEE International Conference on Acoustics, Speech and Signal Processing*, May 2019, pp.2307-2311.

[13] Popescu A C, Farid H. Exposing digital forgeries by detecting traces of resampling. *IEEE Transactions on Signal Processing*, 2005, 53(2): 758-767.

[14] Ianeva T I, de Vries A P, Röhrig H. Detecting cartoons: A case study in automatic video-genre classification. In *Proc. the 2003 IEEE International Conference on Multimedia & Expo*, July 2003, pp.449-452.

[15] Pan F, Chen J, Huang J. Discriminating between photorealistic computer graphics and natural images using fractal geometry. *Science in China Series F: Information Sciences*, 2009, 52(2): 329-337.

[16] Zhang R, Wang R D, Ng T T. Distinguishing photographic images and photorealistic computer graphics using visual vocabulary on local image edges. In *Proc. the 10th International Workshop on Digital Forensics and Watermarking*, October 2012, pp.292-305.

[17] Li Z, Ye J, Shi Y Q. Distinguishing computer graphics from photographic images using local binary patterns. In *Proc. the 11th International Workshop on Digital Forensics and Watermarking*, October 2012, pp.228-241.

[18] Ojala T, Pietikäinen M, Maenpaa T. Multiresolution gray-scale and rotation invariant texture classification with local binary patterns. *IEEE Transactions on Pattern Analysis and Machine Intelligence*, 2002, 24(7): 971-987.

[19] LeCun Y, Bengio Y, Hinton G. Deep learning. *Nature*, 2015, 521(7553): 436-444.

[20] Zhang X J, Lu Y F, Zhang S H. Multi-task learning for food identification and analysis with deep convolutional neural networks. *Journal of Computer Science and Technology*, 2016, 31(3): 489-500.

[21] Cheng M M, Hou Q B, Zhang S H, Rosin P L. Intelligent visual media processing: When graphics meets vision. *Journal of Computer Science and Technology*, 2017, 32(1): 110-121.

[22] Quan W, Yan D M, Guo J, Meng W, Zhang X. Maximal Poisson-disk sampling via sampling radius optimization. In *Proc. the SIGGRAPH ASIA*, December 2016, Article No. 22.

[23] Barnes C, Zhang F L. A survey of the state-of-the-art in patch-based synthesis. *Computational Visual Media*, 2017, 3(1): 3-20.

[24] Hinton G E, Krizhevsky A, Wang S D. Transforming auto-encoders. In *Proc. the 21st International Conference on Artificial Neural Networks*, June 2011, pp.44-51.

[25] Sabour S, Frosst N, Hinton G E. Dynamic routing between capsules. In *Proc. the 2017 Annual Conference on Neural Information Processing Systems*, December 2017, pp.3856-3866.

[26] Tarianga B D, Senguptab P, Roy A, Chakraborty R S, Naskar R. Classification of computer generated and natural images based on efficient deep convolutional recurrent attention model. In *Proc. the IEEE Conference on Computer Vision and Pattern Recognition Workshops*, June 2019, pp.146-152.

[27] Yan Y, Ren W, Cao X. Recolored image detection via a deep discriminative model. *IEEE Transactions on Information Forensics and Security*, 2019, 14(1): 5-17.

[28] Bottou L. Large-scale machine learning with stochastic gradient descent. In *Proc. the 19th International Conference on Computational Statistics*, August 2010, pp.177-186.

[29] Dang-Nguyen D T, Pasquini C, Conotter V, Boato G. RAISE: A raw images dataset for digital image forensics. In *Proc. the 6th ACM Multimedia Systems Conference*, March 2015, pp.219-224.

[30] Ng T T, Chang S F, Hsu J, Pepeljugoski M. Columbia photographic images and photorealistic computer graphics dataset. Technical Report, Department of Electrical Engineering, Columbia University, 2004. http://www.ee.columbia.edu/ln/dvmm/publications/05/ng_cgdataset_05.pdf, Jan. 2019.

[31] Gunturk B K, Altunbasak Y, Mersereau R M. Color plane interpolation using alternating projections. *IEEE Transactions on Image Processing*, 2002, 11(9): 997-1013.

Rui-Song Zhang is currently pursuing his M.S. degree in the National Laboratory of Pattern Recognition (NLPR), Institute of Automation, Chinese Academy of Sciences, Beijing. He received his B.S. degree in information security from Xidian University, Xi'an, in 2019. His research interests include image processing and image forensics.

Wei-Ze Quan received his B.S. degree in electronic information engineering from Wuhan University of Technology, Wuhan, in 2014, and he is currently a Ph.D. candidate in National Laboratory of Pattern Recognition (NLPR), Institute of Automation, Chinese Academy of Sciences, Beijing. His research interests include geometry processing and image forensics.

Lu-Bin Fan is a senior algorithm engineer at Alibaba Group, Hangzhou. He received his B.Sc. and Ph.D. degrees in mathematics from Wuhan University, Wuhan, in 2009, and Zhejiang University, Hangzhou, in 2014, respectively. From 2014 to 2017, he was a postdoctoral fellow at the Visual Computing Center, King Abdullah University of Science and Technology (KAUST). He joined the Alibaba Group in 2017. His research interests include image and video processing, geometric processing and procedural modeling.

Li-Ming Hu is a professor at the State Key Laboratory of Hydro-Science and Engineering, Department of Hydraulic Engineering, Tsinghua University, Beijing. He received his Ph.D. and Bachelor's degrees in hydraulic engineering from Tsinghua University, Beijing, in 2000 and 1995, respectively. His research interests include unsaturated soil mechanics, soil-structure interaction, and contaminated site remediation.

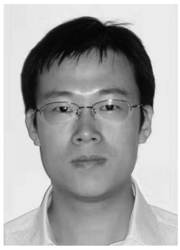

Dong-Ming Yan is a professor at the National Laboratory of Pattern Recognition of the Institute of Automation, Chinese Academy of Sciences (CAS), Beijing. He received his Ph.D. degree in computer science from Hong Kong University, Hong Kong, in 2010 and his Master's and Bachelor's degrees in computer science from Tsinghua University, Beijing, in 2005 and 2002, respectively. His research interests include computer graphics, computer vision, geometric processing and pattern recognition.